Spatial mode projection for side-wall angle measurements

L. Cisotto, Y. Zhu, S. F. Pereira and H. P. Urbach

Optics Research Group, Dept. of Imaging Physics, Delft University of Technology,
van der Waalsweg 8, 2628 CH, Delft, The Netherlands

ABSTRACT

Finding a fast and precise method to measure the side-wall angle of periodic (or non-periodic) structures is still a very challenging problem in lithographic applications. For this reason, over the years, many techniques have been proposed to circumvent this limitation, with the final goal to give the most precise geometrical description of particular targets. Recently, the investigation of the optical angular momentum, which is encoded in the light's spiral spectrum, has brought new ways to acquire information about objects. In this work, we built an optical setup to put forward a new method to detect the side-wall angle in a fast and reliable way. The novelty of this work is the use of the spiral spectrum of a light beam for angle measurements, i.e. the light transmitted by a particular structure is projected onto properly tailored spatial modes and only the most sensitive mode to the side wall angle is detected and processed.

Keywords: Side-wall angle, orbital angular momentum, mode expansion, spiral spectrum

1. INTRODUCTION

Nowadays, the demand for faster, smaller and lighter electronic devices sets stringent requirements for nano-lithography.[1] In particular, modern electronic chips can be modeled with optical gratings, which can be described by four different shape parameters that fully characterize their geometrical profile, namely MidCD (Middle Critical Dimension), SWA (side-wall angle), height and pitch. The knowledge of these parameters is a key factor to fabricate chips accordingly to the initial design; the better the error estimation of their values, the more devices will behave as predicted. Different inspection techniques can be used to retrieve the shape parameters, for instance SEM and AFM. Nevertheless, scatterometry is often a valid alternative because it is a fast and non-destructive technique, and it does not suffer from the Rayleigh diffraction limit. Using this method and a coherent light source, it has been already proved experimentally[2] that it is possible to retrieve, with very high sensitivity, the values of the aforementioned parameters; nonetheless, regarding the side-wall angle (SWA) measurement, the uncertainty is still quite large compared to the other quantities, thereby making conventional detection techniques not very appealing for its determination. As a consequence, over the years several methods have been designed to measure, as precisely as possible, the SWA value.[3–5] Available techniques try to exploit all the fundamental properties of light, e.g. the energy spectra and the energy density of light signals, but in the past few years much attention has been given to the study of the interaction between angular momentum and matter. It is indeed known that angular momentum can contain not only a spin contribution, associated to the polarization of the electromagnetic fields, but also an orbital contribution associated to the spatial profile of the light beam amplitude and phase-front.[6,7] Furthermore, it is possible, within the paraxial regime, to decouple them.[8–10] An important difference between the spin angular momentum and the orbital angular momentum is that the former manifests itself in the vectorial nature of a light field and is thus sensitive to material anisotropies; conversely, the orbital angular momentum can be associated to the topological properties of a light field and hence it is sensitive to phase gradients and discontinuities. It is interesting to observe that in the past years, the orbital contribution has resulted in important applications in fields that range from optical tweezers in biosciences, to microfluidics and micromechanics.[11–14]

We present here a new way that could potentially increase the precision of the SWA detection, while keeping the experimental setup fast and non-invasive. The key point is to look at the spectral content of a light

---

Further author information: (Send correspondence to L. Cisotto)
E-mail: l.cisotto@tudelft.nl, Telephone: +31 (0)15 27 89407

beam, using a technique called *spatial mode projection*. The potential of this approach has already been demonstrated[15, 16] and it has also been used to determine, with incredible precision, the height of thin nanolayers.[17] In this technique, the target is illuminated with a light beam presenting a convenient spatial shape (amplitude and phase), and the reflected (or transmitted) signal is then expanded into spiral eigenstates of orbital angular momentum; information regarding the target can be acquired by analyzing the corresponding spiral spectrum. The sample studied here is simply a phase step, to elucidate the simplicity and power of our technique.

2. THEORY

It is well known that a light beam carrying Orbital Angular Momentum (OAM) can be written in terms of Laguerre-Gaussian (LG) beams, described by the following profile (at its waist):

$$LG_{p,m}(r,\theta) = \sqrt{\frac{2\,p!}{\pi(p+|m|)!}}\,\frac{1}{w_0}\,\left(\frac{r\sqrt{2}}{w_0}\right)^{|m|} L_p^{|m|}\left(\frac{2\,r^2}{w_0^2}\right)\exp\left(-\frac{r^2}{w_0^2}\right)\exp\left(im\theta\right) \tag{1}$$

where the symbol $L_p^{|m|}$ stands for the Laguerre polynomials and w_0 is the waist size. Their amplitude and phase profile is characterized by two integer numbers, usually labeled as p and m. The former can take any nonnegative value and determines the radial shape (and therefore the node number) of the beam distribution; the latter, which can take any integer number, describes the azimuthal phase dependence of the mode. When $m \neq 0$, the LG modes contain optical vortices, with topological charge, or winding number, given by m itself. We notice that in the case $p = m = 0$ the light profile is nothing but the simple Gaussian beam. The Laguerre-Gaussian functions are a complete orthonormal set of functions; in fact we can introduce the following inner product for the Laguerre polynomials:

$$\int_0^{+\infty} L_m^\alpha(x)\,L_n^\alpha(x)\,d\mu(x) = \frac{\Gamma(m+\alpha+1)}{m!}\,\delta_{n,m} \qquad \text{with} \quad d\mu(x) = x^\alpha e^{-x}dx \tag{2}$$

by defining the functions $\psi_m(x) = x^{\alpha/2}e^{-x/2}L_m^\alpha(x)$ and $\psi_n(x) = x^{\alpha/2}e^{-x/2}L_n^\alpha(x)$ we get:

$$\int_0^{+\infty} \psi_n(x)\,\psi_m^*(x)\,dx \quad \in L^2\left(\mathbb{R}\right). \tag{3}$$

It is easy to see that if $x = 2\,r^2/w_0^2$ and $\alpha = |m|$ the function $\psi_n(x)$ represents exactly the Laguerre-Gaussian modes. This property allows us to expand any field as a vector state in that basis. In this way, we can look at the spiral decomposition of any given input field and, for instance, observe its change after the interaction with a sample. By looking at how each individual mode gets modified by the presence of an object, we can infer, and therefore quantify, important properties that define it. In the limit of paraxial optics, it is possible to project a generic field $f(r,\theta)$ into the spiral harmonics $\exp\left(im\theta\right)$ using a rather simple expression; this accounts for the weight of all the LG modes with identical azimuthal number m, independently of the radial number p:

$$f(r,\theta) = \frac{1}{\sqrt{2\pi}}\sum_{m=-\infty}^{m=+\infty} a_m(r)\,\exp\left(im\theta\right). \tag{4}$$

where:

$$a_m(r) = \frac{1}{\sqrt{2\pi}}\int_0^{2\pi} f(r,\theta)\,\exp\left(-im\theta\right)d\theta \tag{5}$$

(r,θ) are coordinates in the transverse plane and $a_m(r)$ describes the radial dependence associated with every spiral mode. In this work, we are interested in the analysis, in the limit of paraxial optics, of the interaction between a phase object and an input beam; this means that such a target will mainly act on the overall phase of the beam which is passing through it, leaving its amplitude almost unchanged. The scatterer, in our model, is a step with a specific height and side-wall angle (SWA) that has been studied both theoretically and experimentally. Our goal is to retrieve particular shape parameters of the sample by exploiting the OAM change during the interaction between the light and the scatterer. The procedure we applied is similar to a previous work,[16]
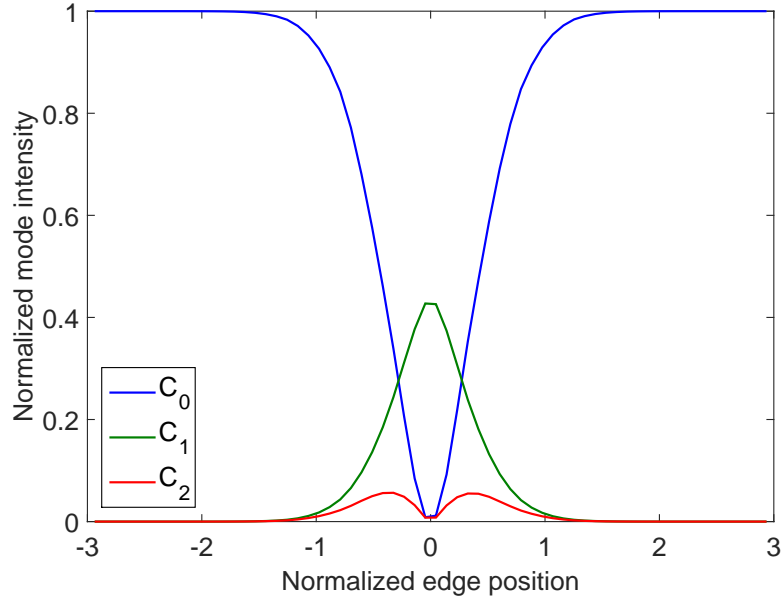
Figure 1. Mode power as function of the edge position normalized to the waist of the beam for a perfect $90°$ edge at the center of the beam, for a π phase shift.

although in our case the detection of the zeroth order mode is used to estimate a specific parameter, namely the side-wall angle. The expression of the energy content (weight) carried by a generic mode m is:

$$P_m = \frac{c_m}{\sum_q c_q} \tag{6}$$

in which $c_m = |\int_0^{+\infty} a_m(r)\, r\, dr|^2$. The weight of the first three modes, corresponding to $m = 0, 1, -1$, are plotted in Fig.1; it can be readily seen that the zeroth order mode presents the biggest change when we scan the sample in a direction perpendicular to the beam; we therefore believe it's more practical to monitor the signal corresponding to this mode. It is also worth mentioning that the angular momentum of the light beam can be expressed as $L_z = (2\epsilon_0/\omega) \sum_{-\infty}^{+\infty} m\, c_m$. Therefore, the simple evaluation of c_m provides information about the beam even if the total orbital angular momentum is zero.

3. SIMULATION

Firstly, we studied the interaction between a phase object and a light beam from a numerical point of view. Hence, we considered an input beam consisting of a collimated Gaussian beam (for the reasons stated in the previous section), which interacts with an object designed to give a phase shift of π in transmission. The beam resulting from the interaction with the scatterer, is then expanded into its spiral spectrum, and the power corresponding to the $m = 0$ mode is detected. Ideally, the target will be made of a substrate on top of which we deposit a layer of a desired material that covers part of the sample; its height will be chosen accordingly to the phase change we want to imprint in the incoming beam. Nonetheless, fabrication processes always give a trade-off with the designed parameters we hope to achieve. As a result, the coated layer will not present a sharp and abrupt profile, but rather a smoother contour with rounded edges and an unknown side-wall angle. This behavior can be taken into account theoretically if the sample is modeled with the following function:

$$\phi_t(x) = \frac{h}{2} \left(1 + \text{erf}\left(t\,\sqrt{\pi}\,\frac{x}{h}\right)\right) \tag{7}$$

where the symbol erf represents the Gaussian Error Function defined by:

$$\text{erf}(x) = \frac{2}{\sqrt{\pi}} \int_0^x e^{-s^2}\, ds, \tag{8}$$
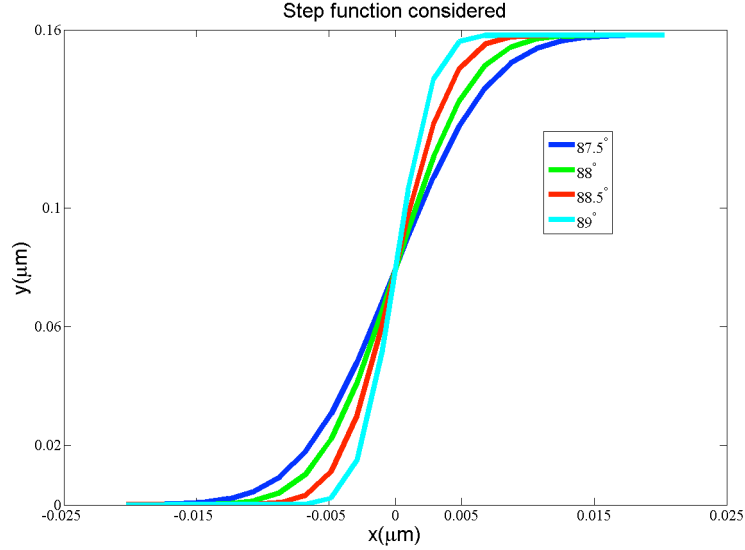
Figure 2. Step function for different SWA values

h and t represent the height of the step and a direct link to the slope of this function, respectively. In fact, the first derivative of this function is given by $t \exp(-x^2)$, hence its slope - in other words, the side-wall angle - varies with the parameter t in a neighboring region of zero. To visualize this function, a plot of $\phi_t(x)$ is given in Fig. 2 for several values of the parameter t. The transmission function of the target will be:

$$T(r, \theta, x_0) := \begin{cases} \beta \, \exp(ik\phi_t(x)), & \text{if} \quad r\cos(\theta) > x_0 \\ 1, & \text{if} \quad r\cos(\theta) \leqslant x_0 \end{cases} \tag{9}$$

where β is the modulus of the transmittance of the object and x_0 corresponds to the position of the edge of the sample. We immediately notice that, to get a phase shift of π in transmission, the optical path difference between the portion of the beam that goes through the step and its surroundings should be $\lambda/2$, with λ being the wavelength in air. In the case where the input Gaussian beam is represented by the function $LG_{0,0}(r, \theta)$, the beam that exits the target will simply be $U(r, \theta, x_0) = LG_{0,0}(r, \theta) \, T(r, \theta, x_0)$. Subsequently, using Eqs. 4 and 5, we get the spiral decomposition. In particular, the expression for the radial dependence is:

$$a_m(r) = \frac{1}{\sqrt{2\pi}} \int_0^{2\pi} LG_{0,0}(r, \theta) \, T(r, \theta, x_0) \, \exp(-im\theta) \, d\theta \, . \tag{10}$$

This is subsequently inserted into the expression of c_m.

The beam is scanned orthogonally to the sample and, for every position, the intensity is detected, a sketch of this procedure is given in Fig. 3 for clarification. The total intensity profile we obtain, looking at the zeroth order, is given in Fig. 4. The plotted intensity profile has been obtained with the following input parameters $\beta = 0.94$, $h = 304 \, nm$, $t = 0.0029 \rightarrow \text{SWA} = 0.16°$. Furthermore, the x-axis has been normalized to the waist value. The curve is not symmetric around the center because of the presence of the β coefficient in one of the two sides of the transmission function $T(r, \theta, x_0)$. The model developed in this section will be used as best fit for the experimental data.

4. EXPERIMENT AND DISCUSSION

The following step was to verify experimentally the numerical results obtained with the simulations. We therefore have built an experimental setup to test the predictions given by the numerical analysis for the case of a Gaussian input beam. A schematic representation of the optical setup is given in Fig. 5. A He:Ne laser illuminates a sample
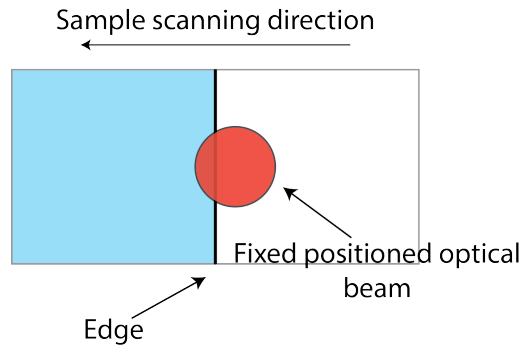
Figure 3. Sketch of the scanning procedure performed during data acquisition.
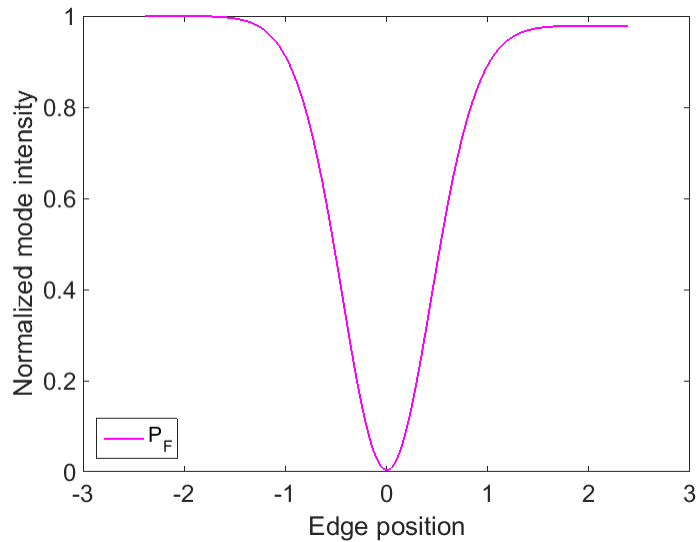
Figure 4. Numerical intensity profile for the zeroth order mode as a function of the position of the beam with respect to the step.

(S) made of a glass substrate with a coated area which covers approximately one half of the total available surface; the material used in this process is silicon nitride (refractive index of 2.01 at $633\,nm$) and the layer thickness is $304\,nm$. The specimen is mounted in a translation stage that allows to scan the y direction. The sample is optically conjugated to a fiber collimator by means of a $4f$ system (lenses L_1 and L_2), in which either lenses have a focal length of $10\,cm$. Subsequently, a single mode fiber (SMF) sends the signal to a photodetector (PD) that is connected to a low noise current amplifier (A). The amplifier is needed because of the very low value of the intensity of the signal when the half of the Gaussian input beam experiences a π phase shift. The amplifier is then connected to an oscilloscope (not represented in the figure) to monitor the voltage. The phase conjugation
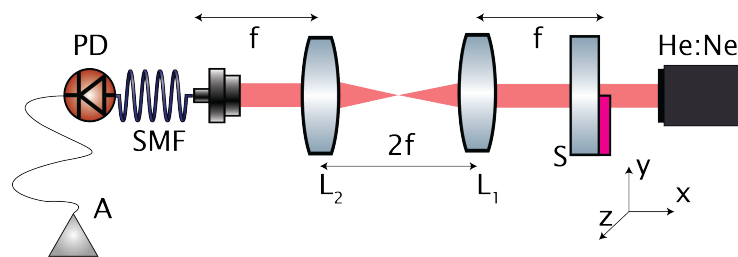
Figure 5. Sketch of the experimental setup

between the sample and the fiber collimator is crucial, we need to reduce phase aberrations due to propagation as much as possible, since the whole detection concept is based on the phase change that the input beam experiences while interacting with the object. With this setup, we can link the position of the sample with the voltage measured by the detection system. The profile of the step sample has been also measured independently with a profilometer, and the obtained data has been fit with Eq. 7, as it is shown in Fig.6, obtaining the following set of parameters $h = 290\,nm$, $t = 0.0029 \rightarrow \text{SWA} = 0.17°$. As represented in the sketch of the experimental
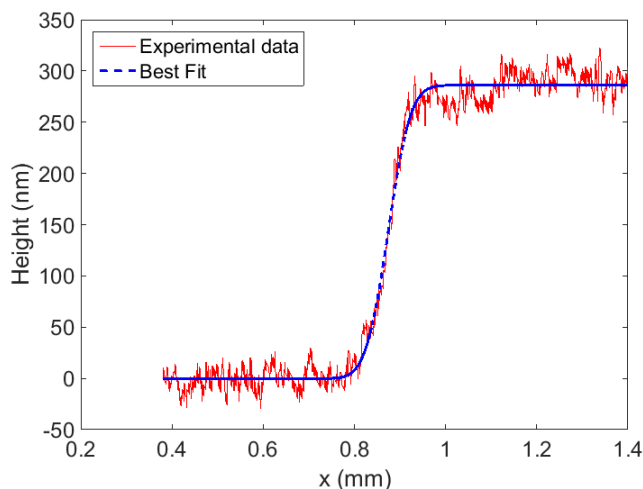
Figure 6. Profilometer data and best fit

setup, the beam is coupled to a single mode fiber after the interaction with the sample, and hence we have to project it onto the Gaussian mode of the fiber. We used two identical fiber collimators to shine light on the target and couple it onto the SMF; this allows us to assume that the beam width does not change significantly over the propagation distance and gives us the normalization constant $N = 2/\pi\,w^2$. The detected power is therefore given by:

$$P_F = \left| \frac{2}{w^2\pi} \int_0^{+\infty} a_0(r)\,r\,dr \right|^2 . \tag{11}$$

The optimized parameters are obtained by fitting the acquired with this equation, where the starting guess given by the parameters derived by fitting the profilometer data. The accuracy of the best fit is influenced both by the experimental data and the profilometer data. The red line in Fig. 7 represents the profile obtained by moving the sample in a direction orthogonal to the beam propagation (y direction). As we can see, the edges are the most problematic part; they are characterized by intensity oscillations and, particularly for positive values of the edge position, the behavior does not resemble the best fit in Fig. 4 (obtained from the function ϕ_t in Eq. 7). Possible explanations for this discrepancy might be found in the fact that the laser has some intensity fluctuations. Moreover, the alignment of the optical components is of great importance, especially the coupling of the beam into the single mode fiber. It is worth noticing that the experimental and theoretical data are in a good agreement for negative scan values, whereas some differences appear for positive values, precisely on the half of the coated surface. In fact, the sample was mainly designed to give an overall π phase shift in transition for a large beam illuminating it, not for side-wall angle measurements, therefore irregularities in the coating might be the cause of the different behavior between experiment and theory. Table 1 summarizes all the values we measured so far, i.e. height measurement made with an ellipsometer, height and side-wall angle made with a profilometer. Only the height value obtained from the profilometer fit is very different from the others, nevertheless, looking at Fig. 6, we notice that the asymptotic value seems to be close to $300\,nm$. Furthermore, the presence of noise affects the accuracy of the fit.
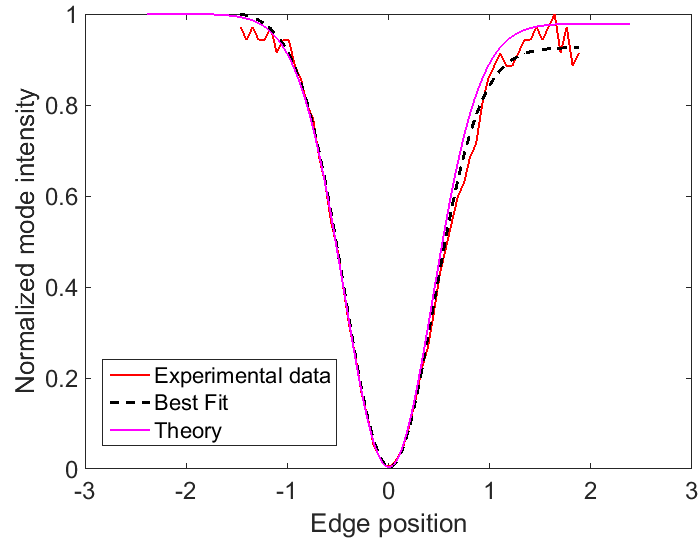
Figure 7. Plot of the obtained experimental data and best fit, along with theoretical prediction using the parameters given by the best fit.

Table 1. Best fit parameters from the profilometer and measured data.

	Profilometer fit	Experimental fit	Ellipsometer
$h\,(nm)$	290 ± 2	308 ± 93	304
SWA($^\circ$)	0.170 ± 0.007	0.16 ± 0.13	

5. CONCLUSIONS

In this work, we have presented a simple and intuitive experimental setup to measure the side-wall angle of a target, consisting of a phase jump designed to give a phase shift of π in transmission. We have theoretically modeled the sample to account for round edges, which are usually formed during fabrication processes, thus implementing a more realistic analysis. For the case of a shallow profile, we were able to determine with good accuracy the value of the side-wall angle by fitting the experimental data with the predictions given by the theoretical model. Successful implementation of this concept for the determination of extremely sharp side-wall angles, might have important and noticeable applications in the field of surface metrology.

ACKNOWLEDGMENTS

REFERENCES

[1] "International technology roadmap for semiconductors," (2012). Available from http://www.itrs.net/Links/2012ITRS/2012Chapters/2012Overview.pdf.

[2] Kumar, N., Petrik, P., Ramanandan, G. K. P., Gawhary, O. E., Roy, S., Pereira, S. F., Coene, W., and Urbach, H. P., "Reconstruction of sub-wavelength features and nano-positioning of gratings using coherent fourier scatterometry," *Optics Express* **22**(20), 24678–24688 (2014).

[3] Martin, Y. and Wickramasinghe, H. K., "Method for imaging sidewalls by atomic force microscopy," *Appl. Phys. Lett.* **64**, 2498 (1994).

[4] Hu, T., Jones, R. L., li Wu, W., Lin, E. K., Lin, Q., Keane, D., Weigand, S., and Quintana, J., "Small angle x-ray scattering metrology for sidewall angle and cross section of nanometer scale line gratings," *Appl. Phys. Lett.* **96**, 1983 (2004).

[5] Su, B., Pan, T., Li, P., Chinn, J., Shi, X., and Dusa, M., "Sidewall angle measurements using CD SEM," in [*Advanced Semiconductor Manufacturing Conference and Workshop*], 259–261, IEEE, Boston (MA) (1998).

[6] Allen, L., Padgett, M. J., and Babiker, M., "The orbital angular momentum of light," *Progress in Optics* **39**, 291–372 (1999).

[7] Padgett, M. J., Courtial, J., and Allen, L., "Light's orbital angular momentum," *Phys. Today* **57**, 35–40 (2004).

[8] Cohen-Tannoudji, C., Dupont-Roc, J., and Grynberg, G., [*Photons and atoms: Introduction to Quantum Electrodynamics*], Wiley, New York (1989).

[9] Barnett, S. M., "Optical angular-momentum flux," *J. Opt. B* **4**, S7–S16 (2002).

[10] Neil, A. T., MacVicar, I., Allen, L., and Padgett, M. J., "Intrinsic and extrinsic nature of the orbital angular momentum of a light beam," *Phys. Rev. Lett.* **88**, 053601 (2002).

[11] Dholakia, K., Spalding, G., and MacDonald, M., "Optical tweezers: the next generation," *Phys. World* **15**(31) (2002).

[12] Galajda, P. and P.Ormos, "Complex micromachines produced and driven by light," *Appl. Phys. Lett.* **78**, 249–251 (2001).

[13] Ladavac, K. and Grier, D. G., "Microoptomechanical pumps assembled and driven by holographic optical vortex arrays," *Opt. Express* **12**, 1144 (2004).

[14] Voogd, R. J., Singh, M., Pereira, S., van de Nes, A., and Braat, J., "The use of orbital angular momentum of light beams for super-high density optical data storage," in [*OSA annual meeting*], (2004).

[15] Torner, L., Torres, J. P., and Carrasco, S., "Digital spiral imaging," *Opt. Express* **13**(3), 873–881 (2005).

[16] Molina-Terriza, G., Rebane, L., Torres, J. P., Torner, L., and Carrasco, S., "Probing canonical geometrical objects by digital spiral imaging," *J. Europ. Opt. Soc. Rap. Public.* **2**, 07014 (2007).

[17] Hermosa, N., Rosales-Guzman, C., Pereira, S. F., and Torres, J. P., "Nanostep height measurements via spatial mode projection," *Opt. Lett.* **39**(2), 299–302 (2014).